UC San Diego

UC San Diego Previously Published Works

Title

Cell Adhesiveness Serves as a Biophysical Marker for Metastatic Potential

Authors

Beri, Pranjali
Popravko, Anna
Yeoman, Benjamin
et al.

Cell adhesiveness serves as a biophysical marker for metastatic potential

Pranjali Beri[1], **Anna Popravko**[1], **Benjamin Yeoman**[1,4], **Aditya Kumar**[1], **Kevin Chen**[1], **Enio Hodzic**[1], **Alyssa Chiang**[1], **Afsheen Banisadr**[2], **Jesse K. Placone**[1,†], **Hannah Carter**[3,4], **Stephanie I. Fraley**[1,4], **Parag Katira**[5,6], **Adam J. Engler**[1,2,7,‡]

[1]Department of Bioengineering, University of California, San Diego; La Jolla, CA 92093 USA

[2]Biomedical Sciences Program, University of California, San Diego; La Jolla, CA 92093 USA

[3]Department of Medicine/Division of Medical Genetics, University of California, San Diego; La Jolla, CA 92093 USA

[4]Moores Cancer Center, University of California, San Diego; La Jolla, CA 92093 USA

[5]Department of Mechanical Engineering, San Diego State University; San Diego, CA 92182 USA

[6]Computational Sciences Research Center, San Diego State University; San Diego, CA 92182 USA

[7]Sanford Consortium for Regenerative Medicine; La Jolla, CA 92037 USA

Abstract

Tumors are heterogeneous and comprised of cells with different dissemination abilities. Despite significant effort, there is no universal biological marker that serves as a metric for metastatic potential of solid tumors. Common to disseminating cells from such tumors, however, is the need to modulate their adhesion as they detach from the tumor and migrate through stroma to intravasate. Adhesion strength is heterogeneous even amongst cancer cells within a given population, and using a parallel plate flow chamber, we separated and sorted these populations into weakly and strongly adherent groups; when cultured under stromal conditions, this adhesion phenotype was stable over multiple days, sorting cycles, and common across all epithelial tumor lines investigated. Weakly adherent cells displayed increased migration in both 2D and 3D migration assays; this was maintained for several days in culture. Subpopulations did not show differences in expression of proteins involved in the focal adhesion complex but did exhibit intrinsic focal adhesion assembly as well as contractile differences that resulted from differential expression of genes involved in microtubules, cytoskeleton linkages, and motor activity. In human breast tumors, expression of genes associated with the weakly adherent population resulted in worse progression-free and disease-free intervals. These data suggest that adhesion strength could potentially serve as a stable marker for migration and metastatic potential within a given tumor

---

‡Corresponding Author: aengler@ucsd.edu, Phone: 858-246-0678, Fax: 858-534-5722.
†Current Affiliation: Department of Physics and Engineering, West Chester University; West Chester, PA 19383 USA

Disclosure of Potential Conflicts of Interest

No potential conflicts of interest were disclosed.

population and that the fraction of weakly adherent cells present within a tumor could act as a physical marker for metastatic potential.

Keywords

Epithelial Cancer; Migration; Shear Stress; Fluid Flow; Heterogeneity

Classification

Biophysical Technologies; Breast Cancer; Lung Cancer

Introduction

The high mortality rate associated with cancer is due to metastasis from a primary tumor to a distal site (1, 2). Patient outcomes typically scale with rate of cell dissemination from the tumor, resulting in lower five-year survival rates for aggressive tumors such as invasive ductal carcinoma (1). However, determining cell dissemination rate from a tumor is difficult due to heterogeneity, *i.e.* cells in the same tumor have different propensities for forming secondary metastases (3-5). Furthermore, there are no universal biochemical markers that predict metastatic potential across solid tumors (4, 6); next generation assays that use these biomarkers typically only surveil cells post-intravasation.

Biophysical markers, such as cell deformability, are an emerging alternative to assess metastatic potential (7-12). Assays based on these metrics focus largely on characterizing the physical properties of already circulating cells rather than understanding how cancer cells physically interact with and adhere to the extracellular matrix (ECM) at the onset of invasion. Given that all cancer cells must interact with the ECM to initiate metastasis, understanding variations in these interactions can serve as an early indicator of metastatic ability. For optimal cell migration into adjacent parenchyma, cells must turnover their focal adhesions to move through the tissue effectively; extremely unstable or stable adhesion can arrest migration as the cell can never establish contractile forces or unbind and retract rear portions of the cell (13). Thus, migration speed is a function of the strength of attachment and is maximized when migrating cells can cycle their adhesions (13, 14). Indeed, invasive cancer cells have more dynamic focal adhesions than their non-invasive counterparts (15), and decreased adhesion strength corresponds to increased metastatic potential (16). As a result, the adhesion of cancer cells to ECM proteins is becoming an accepted metric for metastatic potential (17, 18).

Many assays have been developed to demonstrate how adhesion differs in metastatic cells compared to their non-metastatic counterparts (17, 19-21). However, such assays are either low throughput or not quantitative. It is also difficult to assess adhesive heterogeneity within a single cancer line using these methods (22). We have previously demonstrated that metastatic breast cancer cells display lower cell-ECM adhesion strength than their non-metastatic counterparts using a spinning-disk shear assay (23, 24), especially when cells are exposed to an environment whose low cation concentration mirrors stroma (25, 26). We also observed an inherent heterogeneity in adhesion strength in multiple lineages including

breast, prostate, and lung cancer cell lines (23). Given this information, we developed a parallel plate flow chamber to isolate distinct fractions of cells from a heterogeneous population. Cells were isolated by applying a uniform shear stress to the cell population in the presence of stromal concentrations of Mg and Ca cations (25, 26). Within a given tumor line, we observed significant adhesion heterogeneity and found that the more weakly adherent fraction displays increased migration in both 2D and 3D. This is due to the increased contractility and focal adhesion disassembly present in weakly adherent cells, resulting from transcriptomic expression differences in cytoskeletal components. Together, these data suggest that intrinsic differences in adhesion strength of cells within a population can act as markers of intratumoral heterogeneity in metastatic potential and be exploited to biophysically fractionate subpopulations.

Materials and Methods

Cell Culture:

MDA-MB231 and MCF7 cells were cultured in DMEM, 10% Fetal Bovine Serum (FBS), and 1% antibiotic/antimycotic; MCF10A and MCF10AT cells were cultured in DMEM/F-12, 5% horse serum, 1% penicillin/streptomycin (Pen/Strep), 0.5 μg/ml Hydrocortisone, 20 ng/ml hEGF, 10 μg/ml Insulin, 100 ng/ml Cholera toxin; NCI-H1299 cells were cultured in RPMI, 10% FBS, and 1% Pen/Strep. Products were purchased from Life Technologies. All cells were obtained from ATCC (authenticated by morphology, growth curve, and isoenzyme analysis), verified mycoplasma free via PCR, and were not used beyond passage 10.

Parallel plate shear assay:

Glass plates (Brain Research Laboratories, Waban MA) were sonicated in 70% ethanol and water. Plates were coated with fibronectin at 2 μg/cm^2 for 60 minutes and then blocked with 5% bovine serum albumin for 2 hours at 37°C. Plates are then seeded with cells at a density of 5000 cells/cm^2 and incubated overnight. Components of the parallel plate shear assay (polysulfone base plate, 38 μm thick silicone gasket (SMI), polypropylene luer fixtures (Cole Parmer), 1/8-inch inner diameter tubing (Fisher Scientific)) were assembled and the glass plate was clamped to the base plate containing the inlet and outlet. The inlet tubing was connected to a syringe pump. Shear stress, τ, was calculated using the following equation:

$$\tau = \frac{6\mu Q}{wh^2} \tag{1}$$

Where μ is viscosity of the fluid, Q is volumetric flow rate, w is the width of the chamber, and h is the height of the chamber.

Isolating weakly (WA) and strongly (SA) adherent cells:

To test adhesion stability of WA and SA fractions of the population, we first determined an intermediate shear stress to detach roughly 40% of cells (~170 dynes/cm^2 for MDA-MB231 cells). Phosphate-buffered saline without magnesium and calcium and with 4.5 g/L of

dextrose was used to shear cells. Cells were subjected to the intermediate shear stress for 3 minutes to isolate WA cells in the flow-through, which was collected at the outlet. 0.25% Trypsin-EDTA was added to the device to isolate SA cells. Once cells detached, media was pushed through the device to neutralize the trypsin and remove the SA cells. Both populations were then seeded.

To perform the adhesion stability re-mixed population assay, WA and SA cells were isolated at day 0, cultured separately for 24 hours, re-mixed and seeded onto a plate overnight, then re-isolated at 48 hours after the initial isolation.

To isolate the weakest and strongest 2% of the MDA-MB231 cell population for migration assays, the seeded plate was subjected to a low shear stress (28 dynes/cm^2) for 3 minutes to isolate WA cells in the flow through from the outlet. The shear stress was then increased to a high shear stress (510 dynes/cm^2) for 2 minutes to eliminate intermediate cell fractions. The remaining steps to isolate SA cells are listed above. The weakest MCF10A and MCF10AT cells were isolated using 170 and 130 dynes/cm^2 of shear stress respectively; the strongest were isolated using 1275 and 595 dynes/cm^2 respectively.

Co-culture assay:

MDA-MB231 and MCF10A cells were trypsinized and resuspended in 25 μM of CellTracker fluorescent probes (Molecular Probes, Life Technologies) in serum-free DMEM: MDA-MB231 in Green CMFDA and MCF10A in Orange CMRA. Cell-dye solutions were incubated at room temperature (RT) for 20 minutes. The cells were then centrifuged and resuspended in MDA-MB231 media. Cells were mixed 50:50 and seeded such that the final seeding density was 5000 cells/cm^2, then incubated overnight.

Upon isolation of WA and SA cells, both fractions were seeded, incubated overnight, then fixed the following day with 3.7% formaldehyde for 10 minutes. Cells were imaged using a Nikon Eclipse Ti-S microscope at 10X magnification with FITC and Texas Red and counted by color.

Measuring percent detachment versus metastatic capability:

MDA-MB231, MCF7, MCF10A, and MCF10AT cells were subjected to 250 dynes/cm^2 of shear. The detached and adherent fractions were isolated as described and counted to calculate the fraction of cells detached.

Immunofluorescence staining and focal adhesion (FA) analysis:

Fixed cells were incubated for 10 minutes at RT with CellMask Deep Red plasma membrane stain (1:1000, Thermo Fisher) in 1 mM MgCl$_2$ solution, followed by incubation for 1 hour at RT with blocking solution of 10% goat serum, 0.1% saponin, 1% bovine serum albumin, 0.03 M glycine in 1 mM MgCl$_2$ solution. Primary paxillin antibody (1:250; ab32084, Abcam) in blocking solution was applied overnight at 4°C. Then, a secondary Alexa Fluor 488-conjugated antibody (1:2000, Invitrogen) in blocking solution was applied for 1 hour at RT, followed by Hoechst 33342 (1:2000, Invitrogen) in DI water for 10 min at RT. The cells were subsequently mounted with Fluoromount-G (Southern Biotech). The samples were

imaged with a Zeiss LSM 780 confocal microscope (Zeiss) with a 63x oil-immersion objective. A custom-written ImageJ program was used to quantify cell area and FA number and size. All FA metrics were computed across the entire cell to avoid regional biases.

Traction Force Microscopy (TFM):

Cell tractions were measured as described and calculated using a custom Matlab routine (27). 2% v/v of 0.2 μm diameter 580/605 FluoSpheres microspheres (Invitrogen) were added to the prepolymer solution, comprised of 5% acrylamide, 0.06% bis-acrylamide, 1% ammonium persulfate (Fisher), and 0.1% v/v of N,N,N',N'-Tetramethylethylenediamine (VWR International). Gels were prepared in 12 well glass bottom plates (Cellvis), which were precleaned in a UV/Ozone cleaner (ProCleaner™ Plus, Bioforce Nanosciences) and methacrylated to ensure binding of the gel. Collagen was bound to the surface by adding 0.2 mg/ml sulfo-SANPAH and activating with UV light (wavelength 350 nm) for 10 minutes followed by incubation with 0.15 mg/ml type I collagen. Isolated cells were seeded at ~15,000 cells/cm^2 on the gels and allowed to adhere for 3 hrs. Brightfield images were taken of each cell prior to obtaining microsphere displacements at 60x. Bead reference positions were then re-obtained after removing the cells with a 10% v/v Triton X solution for 10 minutes. Strain energy was determined from the traction stress map and normalized to cell area.

Western blotting:

Weakly and strongly adherent cells were isolated and plated in fibronectin-coated 12-well plates for 3 hours. Cells were lysed with mRIPA supplemented with phosphatase and protease inhibitors as described (28). Protein concentration was measured using a BCA assay. 5 μg protein was mixed with 50 mM DTT, Loading Buffer, and mRIPA, heated at 95°C for 5 minutes, and loaded into a Bolt 4-12% Bis-Tris Plus gel (Invitrogen) and then run with MES running buffer for 30 min at 200 V. Protein was transferred to a nitrocellulose membrane using an iBlot Cell Transfer Stack (Invitrogen). Membrane was blocked with 5% SeaBlock for 1 hour at RT then incubated overnight at 4°C with anti-paxillin (Abcam, ab32084), anti-pFAK (Y397) (Abcam, ab81298), anti-FAK (Origene, TA506161), anti-Actin (Abcam, ab8226), and anti-GAPDH (Abcam, ab8245). The membrane was then incubated for 2 hours at RT with AlexaFluor 680 donkey anti-mouse (Life Technologies, A32788) and AlexaFluor 790 donkey anti-rabbit (Life Technologies, A11374) antibodies. The membrane was imaged using a Li-Cor Odyssey CLx and analyzed using Image Studio Lite (Li-Cor).

2D migration assays on collagen gels:

2.4 mg/mL Type I collagen gels were prepared by mixing collagen (Corning) with PBS, DI water, and 1 M NaOH and adjusted to pH 7.0. Gels were added to a 12-well plates and cured at 37°C for 30 minutes. The weakest and strongest 2% of the cell population were seeded onto the gels and incubated overnight. The cells were imaged with a Nikon Eclipse Ti-S microscope equipped with a temperature- and CO$_2$-controlled stage. Cells were imaged at 10X in brightfield every 15 minutes for 24 hours. The migration data was analyzed via Fiji. The positions were normalized to the starting point and analyzed via a custom MATLAB script to compute instantaneous speed and cell displacement. Cells that divided or did not remain in the frame for 24 hours were not tracked. Cells that interacted with other cells for

more than 2 hours were not tracked, as cell-cell interactions artificially slowed cell speed. For MDA-MB231 cell migration under drug treatment, cells were treated with either 0.2 μg/mL nocodazole (Cayman Chemical) or 0.5 μg/mL paclitaxel (LC Laboratories). Cells were imaged the following day for 24 hours and tracked as stated above.

2D migration assays on polyacrylamide gels of varying stiffness:

Polyacrylamide gels of low and high stiffness were prepared as described in the TFM methods section, without fluorescent microbeads. The high stiffness prepolymer solution has an identical composition to the gels used for TFM, while the low stiffness prepolymer solution consists of 3% acrylamide and 0.06% bis-acrylamide with all other components identical to the high stiffness gel. Cells were isolated, seeded, and tracked as described.

Preparing spheroids of MDA-MB231 cells:

The weakest and strongest 2% of the MDA-MB231 cell population and unselected cells were isolated and seeded in a 12-well plate overnight. Cells were trypsinized and resuspended in 25 μM CellTracker fluorescent probes (Molecular Probes, Life Technologies) as described above. Cells were then centrifuged and resuspended in a solution of 0.25% Methocult in culture media. 2,500 cells (either WA or SA) were added to wells in a 96-well Corning Ultra-Low Attachment Spheroid Microplate (Corning) then incubated for 48 hours.

3D migration assay in collagen gels:

Collagen gels were prepared as described above. Spheroids were embedded in a collagen gel solution and added to a 24-well plate. Media was added to the top of the gel, and a time 0 image was captured at 10X magnification with brightfield to obtain initial radius. Embedded spheroids were incubated for 24 hours, after which they were fixed with 3.7% formaldehyde in solution A for 20 minutes. Spheroids were imaged with a Zeiss LSM 780 Confocal Microscope at 10X magnification with the FITC and Texas Red channel. Z-stack images were acquired at 30 μm intervals from the bottom to the top of the spheroid. Maximum intensity projection images were generated and input into a custom Python script to analyze invasive index of spheroid and maximum displacement of cells in the spheroid. Invasive index is defined as:

$$I = \frac{r_{final}}{r_{initial}} \tag{2}$$

Where $r_{initial}$ is the radius at time t = 0 hours of the spheroid and r_{final} is the radius at time t = 24 hours.

RNA sequencing:

RNA from WA and SA cells was purified using Qiagen RNeasy Mini Kit (Qiagen, 74104). RNA quality was assessed using TapeStation (Agilent), RNA libraries were prepared using the Illumina TruSeq Stranded RNA, High Throughput Library Prep Kit and sequenced using the Illumina HiSeq 4000 system to generate 50 bp single-end reads. Data was analyzed by Rosalind (https://rosalind.onramp.bio/), with a HyperScale architecture developed by OnRamp BioInformatics, Inc. (San Diego, CA). Reads were trimmed using cutadapt (29).

Quality scores were assessed using FastQC (30). Reads were aligned to the Homo sapiens genome build hg19 using STAR (31). Individual sample reads were quantified using HTseq (32) and normalized via Relative Log Expression (RLE) using DESeq2 R library (33). Read Distribution percentages, heatmaps, and sample plots were generated as part of the QC step using RSeQC (34). DEseq2 was also used to calculate fold changes and p-values. Clustering for the differentially expressed gene heatmap was done using the Partitioning Around Medoids method with the fpc R library (35). Functional enrichment analysis of pathways, gene ontology, domain structure and other ontologies was performed using HOMER (36). Enrichment was calculated relative to a set of background genes relevant for the experiment.

Quantitative PCR:

RNA from WA and SA cells was purified using Qiagen RNeasy Mini Kit and reverse transcribed using SuperScript III Reverse Transcriptase (ThermoFisher Scientific, 18080093). Quantitative PCR was performed (45 cycles, 95°C for 15 seconds followed by 60°C for 1 min) using a 7900HT Fast Real-Time PCR System (Thermo Scientific, 4329001) with the primers listed (Supplemental Table S1), and iQ SYBR Green Supermix (Bio-Rad Laboratories, 1708880). Target genes were normalized to GAPDH and mRNA quantity was calculated based on a standard curve generated from a fibronectin plasmid.

TCGA Dataset Analysis:

The TCGA raw data were downloaded from NIH NCI GDC Data portal directly. Corresponding clinical metadata were obtained from a previous publication (37). Only the breast cancer (BRCA) patients with reported negative histological staining for the three markers (Her2, ER, PR) and American Joint Committee on Cancer (AJCC) pathology stages below stage IV were included in our analysis cohort. Patient data were analyzed to determine correlation between gene expression corresponding to weakly adherent or strongly adherent phenotypes and 5-year survival. Patient data were analyzed by normalizing patient gene expression to z-transformed scores with respect to the differentially expressed genes between the weakly adherent and strongly adherent sub-populations. The z-scores were then summed for every patient, and z-score sum-based quantiles were mapped to Strongly Adherent (SA) and Weakly Adherent (WA) categories based on mean gene expression levels. The Kaplan-Meier method was used to create survival plots comparing the 20% of individuals with the lowest score to the 20% with the highest score. The log-rank test was used to determine significance of survival differences between groups. Survival analyses use the Lifelines python library (https://lifelines.readthedocs.io/en/latest/). Relevant scripts for the analysis of TCGA data are available at: https://github.com/kec162ucsd/Tumor-Heterogeneity-Adhesion-Strength/

Statistics:

2D migration assays, 3D spheroid migration assays, and focal adhesion disassembly plots were analyzed using a one-way ANOVA with Tukey test for multiple comparisons. Adhesion stability re-mixed population assay was analyzed with a two-way ANOVA, with Sidak multiple comparison test. All other comparisons were performed using two-tailed unpaired t-test unless otherwise indicated. For all analyses, *$p<0.05$, **$p<0.01$, ***$p<0.001$, ****$p<0.0001$. Data expressed as box-and-whisker plots show all points with the whisker

ends corresponding to minimum and maximum values. All other values are expressed as mean +/− standard deviation. Statistical analyses were performed using Prism software.

Data Availability:

Data generated in this study was deposited to NCBI under GEO GSE135515. We do not impose any restrictions on data availability.

Results

Strongly and weakly adherent phenotypes are maintained post sort

We fabricated a parallel plate flow chamber that exposes cells to discrete, uniform shear stresses in order to isolate fractions of cells based on adhesion strength and study those cells within a heterogeneous population (Figure S1). To ensure that the application of shear did not change the adhesive heterogeneity of the population, we isolated weakly and strongly adherent fractions of MDA-MB231 cells from a parental cell population by exposing the cell to a shear of 170 dynes/cm^2 and stratifying the populations depending on whether they were found in the flow-through or still attached to the device. After sorting, cells were cultured separately, re-mixed, seeded into the device, and subsequently sheared. We found no significant changes between the percent of weakly and strongly adherent cells when tracking cells between days 0 and 2 (Figure 1A), indicating that the parallel plate shear device assesses, but does not alter, the inherent adhesion heterogeneity of the population.

We next wanted to determine if the adhesion phenotype is stably maintained post-isolation. We isolated both fractions from MDA-MB231 cells, cultured them separately in either normal or reduced cation media, and then repeated the isolation on the separated fractions. We found that strongly adherent cells maintained their adherent phenotype 14 days post-isolation, regardless of culture conditions. Weakly adherent cells did not maintain their adhesion phenotype in normal culture media as cells reverted back to their distribution in the parental population; if the selection pressure of low stromal-like cation concentrations was maintained post-isolation, weakly adherent cells were enriched to >70% of the population 6 days post-isolation (Figure 1B).

Parallel plate flow chamber can distinguish between weakly adherent and strongly adherent cell lines.

To test the ability of the flow chamber to select for cells known to have a weaker adhesion strength as a result their higher metastatic potential, MDA-MB231 (metastatic breast cancer line) and MCF10A (non-malignant breast cell line) cells were seeded in a 50:50 mixture and exposed to a shear stress that should detach the MDA-MB231 cells but not the MCF10A cells (170 dynes/cm^2 based on population adhesion assays (23)). The fraction of cells that detached contained 41.7% of the total number of MDA-MB231 cells, while only 0.7% of the total number of MCF10A cells were present in the detached fraction (Figure 1C), consistent with 10-fold higher adhesion strength of MCF10A vs. MDA-MB231 cells in the absence of cations (23) and suggesting that this assay could distinguish metastatic cells from non-cancerous cells.

In order to link quantitative adhesiveness to metastatic potential, we exposed four cell lines of varying metastatic potential (high metastatic capability: MDA-MB231; low metastatic capability: MCF7 and MCF10A; and H-Ras transformed: MCF10AT, which give rise to invasive carcinomas *in vivo* (38)) to 250 dynes/cm^2 of shear stress and counted the fraction of detached cells. As expected, cells with greater tumorigenic and/or metastatic potential had significantly greater detachment at the same shear stress in comparison to cells with lower tumorigenic and/or metastatic potential (Figure 1D).

Weakly adherent cells display greater migratory propensity than strongly adherent cells.

To assess migration differences in adhesion sorted populations, we isolated the ~2% most weakly and most strongly adherent cells of the MDA-MB231 population using 28 dynes/cm^2 and 510 dynes/cm^2, respectively and seeded them onto type-I collagen gels. Over 24 hours post-plating, we found that weakly adherent cells displayed significantly higher average speed than the strongly adherent or unselected (non-sheared) cells (Figure 2A). Weakly adherent cells also displayed increased total cell displacement than the strongly adherent or unselected cells (Figure 2B, Figure S2). Since the adhesion phenotype appears stable, we investigated if migratory differences were stable. Weakly and strongly adherent cells along with unselected population were imaged post selection, and then re-imaged 2 days later. No significant differences for any population were observed post selection or later while the weakly adherent fraction maintained its increased migratory propensity (Figure 2C). The two populations did not exhibit differential proliferation during migration assessments (Figure 2D), suggesting that higher migration speeds for weakly adherent cells were not the result of proliferation differences. In addition to sorting a metastatic population, we further demonstrated sorting fidelity by directly comparing the ~2% most weakly and strongly adherent of MCF10A and isogenic H-Ras transformed MCF10AT cells. Post-sort on collagen gels, we observed that the weakly adherent fraction of MCF10AT cells had increased migration speed and displacement relative to its strongly adherent counterpart, while MCF10A cell fractions did not show differences (Figure S3). These data suggest that heterogeneity in migratory phenotype as a result of selection by adhesion strength is only present in more aggressive cells with increased tumorigenic capability.

Migration can often be affected by matrix properties, and so we sought to determine if migration differences are intrinsic and therefore persist regardless of environmental changes that could reduce substrate adhesion. Weakly and strongly adherent MDA-MB231 cells were plated on polyacrylamide gels of low (300 Pa) and high stiffness (1.8 kPa) and migration observed for 24 hours. Weakly adherent cells were more migratory that the strongly adherent cells independent of substrate stiffness. However, average speed scaled with substrate stiffness gel for both cell fractions, which indicates that both fractions are mechanically sensitive (Figure S4). These results indicate that there are cell intrinsic differences independent of environmental changes that could potentially alter substrate adhesion.

Assays thus far show behaviors in 2D rather than 3D, so we next assessed the outward migration from spheroids containing weakly adherent, strongly adherent or unselected cells (Figure 2E, F). There was no significant difference in maximum cell displacement (Figure 2G), but the leading edge of weakly adherent cells, i.e. the distance at which the signal is

higher than background (Figure S5), migrated further than strongly adherent and unselected cells, indicated by the significantly higher ratio of final radius to initial radius (Figure 2F, H). Consistent with 2D migration, these 3D spheroid data bolster the concept that the fraction of tumor cells with the weakest adhesion most represents those with the highest metastatic potential.

All the cells examined thus far are mammary epithelial, so we next explored whether cells from other epithelial tumors would exhibit the same cation dependent adhesion sorting and migration phenotype. Weakly and strongly adherent NCI-H1299 metastatic lung cancer cells were isolated and their migration analyzed. As with the metastatic mammary tumor line, weakly adherent metastatic lung cancer cells were more migratory than their strongly adherent counterparts (Figure S6), suggesting that this behavior may be universal across epithelial tumors.

Weakly adherent cells have more labile focal adhesions and are more contractile

Migratory differences between weakly and strongly adherent cells did not result from expression differences in focal adhesion proteins, *e.g.* pFAK, FAK, paxillin, or actin (Figure 3A). However, we previously found that metastatic cells preferentially disassemble their focal adhesions relative to non-metastatic cells when exposed to low cation conditions (23). Consistent with this, we found that the strongly adherent subpopulation of MDA-MB231 cells did not fully disassemble focal adhesions after removal of cations. Conversely, weakly adherent cells disassembled their focal adhesions in the absence of cations on fibronectin (Figure 3B-D) or on type I collagen-coated substrates (Figure S7). These data suggest that weak adhesion could be driven by differential sensitivity to cations and could therefore enhance migration. Similarly, cancer cells that exhibit increased contractility are also more migratory than their less contractile counterparts (39, 40). To ascertain if adhesive state is coupled with contractility differences, traction force microscopy was performed on cells post-sort. Weakly adherent cells were significantly more contractile than their strongly adherent counterparts (Figure 3E-F), suggesting that weakly adherent cells represent a more aggressive fraction of the population.

Intrinsic transcriptional variation in microtubule proteins contributes to increased migration of weakly adherent cells.

Given that populations sorted at the less restrictive 170 dynes/cm^2 still remain stable with over 1-2 weeks in culture, and cells sorted at the more restrictive 28 dynes/cm^2 show cell intrinsic migration differences independent of environmental changes that are stable for days in culture, we next interrogated transcriptional differences underlying weakly and strongly adherent phenotypes sorted at 28 dynes/cm^2. Stability appears in part because individual populations do not out compete each other, i.e. cell proliferation rates appear similar (Figure S8). With stable sorting and expansion, we sought to assess differences through post-sort RNA sequencing. Analyses revealed 500 differentially expressed genes between the sub-populations (Figure 4A); replicates clustered by sub-population when comparing differentially expressed genes (Figure 4B). Analysis of genes upregulated in weakly adherent cells demonstrated significant enrichment of gene ontology terms involved in microtubule and cytoskeletal organization and binding (Figure 4C). Genes in these

categories with the most significant expression differences are involved in cytoskeletal components, specifically microtubule-associated proteins. For example, GAS2L3 has been implicated in linking microtubules and actin and results in increased focal adhesion turnover and migration; SYNE2 is also essential for nuclear-cytoskeletal mechano-transduction in invasion and cell contraction (41-43). Components linking the cytoskeleton to the nuclear or plasma membranes were also implicated, *e.g.* AKAP9, which regulates microtubule movement and is highly expressed in highly metastatic cells (44, 45) (Figure 4D). There was also significant enrichment in the expression of motor proteins, specifically those involved in vesicular transport along microtubules (KIF14, DYNC1H1) as well as in cytoskeletal contraction (MYO9A) (Figure 4C-D). KIF14, in particular, is a potent oncogene that is highly expressed in several cancers, particularly breast cancer, and is linked to improved invasiveness and dynamically changing focal adhesions (46, 47). Changes detected through RNA sequencing were validated by qPCR, which confirmed increased expression in weakly adherent cells (Figure 4E).

To functionally confirm a link between the upregulated microtubule components in the weakly adherent cells and their subsequent increased migration, we exposed both weakly and strongly adherent cells to either nocodazole or paclitaxel to dissemble or cap microtubules, respectively. When tracking migration, untreated weakly adherent cells had increased average speed compared to untreated strongly adherent cells. However when treated with either microtubule-targeting drugs, the weakly adherent cells exhibited a significant decrease in average speed, while the strongly adherent cells were unaffected (Figure 4F). These data suggest that inhibiting the microtubule cytoskeleton preferentially impacts the weakly adherent fraction and points to microtubule-affecting agents as potent therapeutic targets.

Finally, we investigated whether differentially expressed genes linked to the highlighted microtubule, cytoskeletal, and microtubule-binding protein ontology terms played a role in human cancer progression. We narrowed the list of genes down to those linked to our highlighted GO terms in Figure 4C, resulting in 100 genes (Supplemental Table 2). Using this gene set, we then analyzed The Cancer Genome Atlas (TCGA) breast cancer dataset and restricted our analysis to triple-negative breast cancer (TNBC) patients with tumors that ranged from Stage I to III. We then compared patients that had gene expression scores that aligned with the strongly and weakly adherent cells. We observed that patients with gene expression profiles similar to the weakly adherent cells had decreased progression-free intervals (Figure 5A) and disease-free intervals (Figure 5B) compared to patients with gene expression profiles similar to the strongly adherent cells. These data suggest that increased expression of genes associated with microtubule and microtubule-binding proteins, as present in the weakly adherent fraction, could define an "adhesive signature" that results in an increase in metastatic potential and promotes human breast tumor progression.

Discussion

Due to the highly heterogeneous nature of tumor cells, both within a given tumor as well as across tumors from different patients, it is difficult to assess tumor aggressiveness and the likelihood of metastasis. In addition, there are no universal biochemical markers that can be

utilized to determine metastatic potential. The emergence of biophysical markers is a new approach to identifying the most aggressive subpopulations of the tumor population. Common cell-ECM interactions of early dissemination of cancer cells of different tumor origins and subsequent ECM deformation reflect the importance of identifying biophysical markers as metrics for metastatic potential (1, 2). To accomplish this, we utilized a parallel plate flow chamber to study the correlation between decreased adhesion strength of cells to ECM proteins and their subsequent metastatic potential. In conjunction with our previous studies (23), we showed that metastatic cancer cells are significantly less adherent than their non-metastatic counterparts. This is demonstrated by the ability to select for MDA-MB231 cells over MCF10A cells from a mixed population. We also found that weak adhesion can serve as a potential marker for metastatic potential, which was demonstrated by the greater percent detachments of MDA-MB231 and MCF10AT cells in comparison to MCF7 and MCF10A cells at the same shear stress.

This study also identified heterogeneity in adhesion strength of cells within a metastatic cancer cell population, especially under stromal-like cation conditions, which may be linked to heterogeneity in metastatic potential of cells within a tumor population and/or circulating tumor cells. This notion is supported by our observations that weakly adherent MDA-MB231 cells exhibited increased migration in comparison to their strongly adherent counterparts. These differences in migration exist in both 2D and 3D environments, which indicates that the weakly adherent subpopulation represents the cells that are more likely to leave the primary tumor and establish secondary metastases (48-50). The stability of this increased migratory propensity for multiple days post-sorting further demonstrates the intrinsic nature of this phenotype. In addition, recapitulating this phenotype in metastatic lung cancer cells suggests that adhesion strength is broadly involved in the more migratory subpopulations within tumors from multiple epithelial backgrounds.

The ability to select this more migratory subpopulation of the cell line stems from differences in focal adhesion disassembly between the weakly adherent and strongly adherent cells. Faster focal adhesion disassembly of weakly adherent cells is consistent with previous findings that link quicker focal adhesion disassembly to more migratory cell lines (15, 51, 52). In addition, weakly adherent cells are more contractile than their strongly adherent counterparts, where increased contractility has also been linked to increased migration and more aggressive cancers (39, 40). Differences in migration, focal adhesion assembly, and contractility can be tied to inherent transcriptomic differences between weakly and strongly adherent cells; genes linked to the cytoskeleton, specifically to microtubules, as well as motor proteins involved in vesicular transport and contraction showed significant differential expression. When we compared human breast cancer patients with gene expression signatures that resembled the weakly and strongly adherent cells for our genes of interest, we observed decreased progression-free and disease-free intervals, implying that tumors resembling the weakly adherent fraction are more aggressive. Several standard cancer therapy drugs (nocodazole, taxols, etc.) target microtubules in order to reduce the growth and spread of aggressive tumors, indicating that differences in microtubules and the cytoskeleton could explain the heterogeneity of tumor cell populations. We confirmed these findings by treating weakly adherent cells to nocodazole and paclitaxel and found that their migration speed reduced to that of the strongly adherent cells, whose

speed was unaffected by both drugs. Therefore, targeting the cytoskeleton is potentially an important method of restricting the motility of highly aggressive subpopulations early in tumor development and suppressing the migratory populations that we observe (53).

This study reveals a strategy to identify distinct subpopulations via shear separation that can be implemented to study the dissemination of cells from a variety of epithelial cancers. Comparing weakly adherent cell populations across multiple metastatic cell lines of various tumor origins could enable the identification of similarities amongst the most aggressive subpopulation in an effort to identify more universal targeted treatments. Lastly, this shear assay can be adapted to study diseases with a similar adhesion component, highlighting the versatility of this technique.

Supplementary Material

Refer to Web version on PubMed Central for supplementary material.

Acknowledgements

References

1. Steeg PS, Targeting metastasis. Nature Reviews Cancer 16, 201–218 (2016). [PubMed: 27009393]

2. L. SR, D. MK, Ahmedin J, Cancer statistics, 2018. CA: A Cancer Journal for Clinicians 68, 7–30 (2018). [PubMed: 29313949]

3. Quintana E et al., Efficient tumour formation by single human melanoma cells. Nature 456, 593 (2008). [PubMed: 19052619]

4. Polyak K, Heterogeneity in breast cancer. The Journal of Clinical Investigation 121, 3786–3788 (2011). [PubMed: 21965334]

5. Sun X.-x., Yu Q, Intra-tumor heterogeneity of cancer cells and its implications for cancer treatment. Acta Pharmacologica Sinica 36, 1219 (2015). [PubMed: 26388155]

6. Liu Y et al., Lack of correlation of stem cell markers in breast cancer stem cells. British Journal Of Cancer 110, 2063 (2014). [PubMed: 24577057]

7. Alibert C, Goud B, Manneville JB, Are cancer cells really softer than normal cells? Biology of the Cell 109, 167–189 (2017). [PubMed: 28244605]

8. Dudani JS, Gossett DR, Tse HTK, Di Carlo D, Pinched-flow hydrodynamic stretching of single-cells. Lab on a Chip 13, 3728–3734 (2013). [PubMed: 23884381]

9. Gossett DR et al., Hydrodynamic stretching of single cells for large population mechanical phenotyping. Proceedings of the National Academy of Sciences of the United States of America 109, 7630–7635 (2012). [PubMed: 22547795]

10. Qi DP et al., Screening cell mechanotype by parallel microfiltration. Scientific Reports 5, (2015).

11. Nyberg KD et al., The physical origins of transit time measurements for rapid, single cell mechanotyping. Lab on a Chip 16, 3330–3339 (2016). [PubMed: 27435631]

12. Beri P et al., Biomaterials to model and measure epithelial cancers. Nature Reviews Materials, (2018).

13. Ridley AJ et al., Cell migration: integrating signals from front to back. Science 302, 1704–1709 (2003). [PubMed: 14657486]

14. DiMilla P, Stone J, Quinn J, Albelda S, Lauffenburger D, Maximal migration of human smooth muscle cells on fibronectin and type IV collagen occurs at an intermediate attachment strength. The Journal of Cell Biology 122, 729–737 (1993). [PubMed: 8335696]

15. Bijian K et al., Targeting focal adhesion turnover in invasive breast cancer cells by the purine derivative reversine. British Journal of Cancer 109, 2810–2818 (2013). [PubMed: 24169345]

16. Indra I et al., An in vitro correlation of mechanical forces and metastatic capacity. Physical Biology 8, (2011).

17. Reticker-Flynn NE et al., A combinatorial extracellular matrix platform identifies cell-extracellular matrix interactions that correlate with metastasis. Nature Communications 3, 1122 (2012).

18. Yates CM, McGettrick HM, Nash GB, Rainger GE, in Metastasis Research Protocols, Dwek M, Schumacher U, Brooks SA, Eds. (Springer New York, New York, NY, 2014), pp. 57–75.

19. Palmer CP et al., Single cell adhesion measuring apparatus (SCAMA): application to cancer cell lines of different metastatic potential and voltage-gated Na+ channel expression. European Biophysics Journal 37, 359–368 (2008). [PubMed: 17879092]

20. Garcia AJ, Gallant ND, Stick and grip. Cell Biochemistry and Biophysics 39, 61–73 (2003). [PubMed: 12835529]

21. Veiseh M et al., Cellular heterogeneity profiling by hyaluronan probes reveals an invasive but slow-growing breast tumor subset. Proceedings of the National Academy of Sciences 111, E1731–E1739 (2014).

22. Gupta Piyush B. et al., Stochastic State Transitions Give Rise to Phenotypic Equilibrium in Populations of Cancer Cells. Cell 146, 633–644 (2011). [PubMed: 21854987]

23. Fuhrmann A, Banisadr A, Beri P, Tlsty TD, Engler AJ, Metastatic State of Cancer Cells May Be Indicated by Adhesion Strength. Biophysical Journal 112, 736–745 (2017). [PubMed: 28256233]

24. Fuhrmann A, Li J, Chien S, Engler AJ, Cation Type Specific Cell Remodeling Regulates Attachment Strength. PLOS ONE 9, e102424 (2014). [PubMed: 25014042]

25. Seltzer MH, Rosato FE, Fletcher MJ, Serum and tissue magnesium levels in human breast carcinoma. J Surg Res 10, 159–162 (1970). [PubMed: 5437734]

26. Seltzer MH, Rosato FE, Fletcher MJ, Serum and tissue calcium in human breast carcinoma. Cancer Res 30, 615–616 (1970). [PubMed: 5425286]

27. Lo Sardo V et al., Unveiling the Role of the Most Impactful Cardiovascular Risk Locus through Haplotype Editing. Cell 175, 1796–1810.e1720 (2018). [PubMed: 30528432]

28. Kumar A et al., Mechanical activation of noncoding-RNA-mediated regulation of disease-associated phenotypes in human cardiomyocytes. Nature Biomedical Engineering 3, 137–146 (2019).

29. Martin M, Cutadapt removes adapter sequences from high-throughput sequencing reads. 2011 17, 3 (2011).

30. Andrews S. (2010).

31. Dobin A et al., STAR: ultrafast universal RNA-seq aligner. Bioinformatics 29, 15–21 (2012). [PubMed: 23104886]

32. Anders S, Pyl PT, Huber W, HTSeq—a Python framework to work with high-throughput sequencing data. Bioinformatics 31, 166–169 (2014). [PubMed: 25260700]

33. Love MI, Huber W, Anders S, Moderated estimation of fold change and dispersion for RNA-seq data with DESeq2. Genome Biology 15, 550 (2014). [PubMed: 25516281]

34. Wang L, Wang S, Li W, RSeQC: quality control of RNA-seq experiments. Bioinformatics 28, 2184–2185 (2012). [PubMed: 22743226]

35. Hennig C.

36. Heinz S et al., Simple Combinations of Lineage-Determining Transcription Factors Prime cis-Regulatory Elements Required for Macrophage and B Cell Identities. Molecular Cell 38, 576–589 (2010). [PubMed: 20513432]

37. Liu J et al., An Integrated TCGA Pan-Cancer Clinical Data Resource to Drive High-Quality Survival Outcome Analytics. Cell 173, 400–416.e411 (2018). [PubMed: 29625055]

38. H. HG, R. WS, MCF-10AT: A Model for Human Breast Cancer Development. The Breast Journal 5, 122–129 (1999). [PubMed: 11348271]

39. Mierke CT et al., Vinculin facilitates cell invasion into three-dimensional collagen matrices. The Journal of biological chemistry 285, 13121–13130 (2010). [PubMed: 20181946]

40. Kraning-Rush CM, Califano JP, Reinhart-King CA, Cellular traction stresses increase with increasing metastatic potential. PloS one 7, e32572–e32572 (2012). [PubMed: 22389710]

41. Stroud MJ, Kammerer RA, Ballestrem C, Characterization of G2L3 (GAS2-like 3), a new microtubule- and actin-binding protein related to spectraplakins. The Journal of biological chemistry 286, 24987–24995 (2011). [PubMed: 21561867]

42. Friedl P, Wolf K, Lammerding J, Nuclear mechanics during cell migration. Current Opinion in Cell Biology 23, 55–64 (2011). [PubMed: 21109415]

43. Jayo A et al., Fascin Regulates Nuclear Movement and Deformation in Migrating Cells. Developmental Cell 38, 371–383 (2016). [PubMed: 27554857]

44. Kumar N, Gupta S, Dabral S, Singh S, Sehrawat S, Role of exchange protein directly activated by cAMP (EPAC1) in breast cancer cell migration and apoptosis. Molecular and Cellular Biochemistry 430, 115–125 (2017). [PubMed: 28210903]

45. Yang M-H et al., MALAT1 promotes colorectal cancer cell proliferation/migration/invasion via PRKA kinase anchor protein 9. Biochimica et Biophysica Acta (BBA) - Molecular Basis of Disease 1852, 166–174 (2015). [PubMed: 25446987]

46. Ahmed SM et al., KIF14 negatively regulates Rap1a–Radil signaling during breast cancer progression. The Journal of Cell Biology 199, 951–967 (2012). [PubMed: 23209302]

47. Thériault BL et al., Transcriptional and Epigenetic Regulation of KIF14 Overexpression in Ovarian Cancer. PLOS ONE 9, e91540 (2014). [PubMed: 24626475]

48. Mi L et al., The metastatic suppressor NDRG1 inhibits EMT, migration and invasion through interaction and promotion of caveolin-1 ubiquitylation in human colorectal cancer cells. Oncogene 36, 4323 (2017). [PubMed: 28346422]

49. Hu J, Verkman AS, Increased migration and metastatic potential of tumor cells expressing aquaporin water channels. The FASEB Journal 20, 1892–1894 (2006). [PubMed: 16818469]

50. Slack JK et al., Alterations in the focal adhesion kinase/Src signal transduction pathway correlate with increased migratory capacity of prostate carcinoma cells. Oncogene 20, 1152 (2001). [PubMed: 11313859]

51. Frame MC, Fincham VJ, Carragher NO, Wyke JA, v-SRC'S hold over actin and cell adhesions. Nature Reviews Molecular Cell Biology 3, 233 (2002). [PubMed: 11994743]

52. McLean GW et al., The role of focal-adhesion kinase in cancer — a new therapeutic opportunity. Nature Reviews Cancer 5, 505 (2005). [PubMed: 16069815]

53. Feng R et al., Targeting the Microtubular Network as a New Antimyeloma Strategy. Molecular Cancer Therapeutics 10, 1886–1896 (2011). [PubMed: 21825007]

Significance

Cancer cells exhibit heterogeneity in adhesivity which can be used to predict metastatic potential.
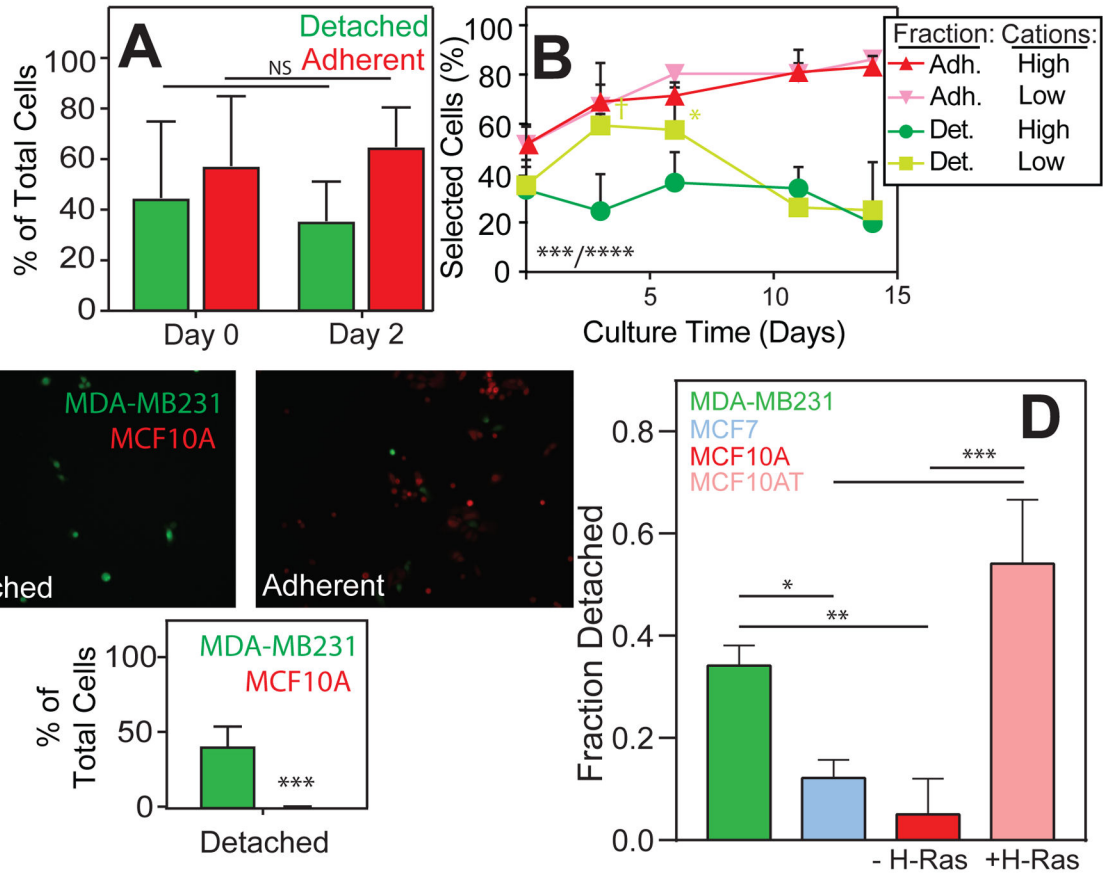
Figure 1: Low Cation PPFC Accurately and Precisely Sorts Cancer Cell Populations that are Stable Long-term.

(A) MDA-MB231 populations were sorted at day 0, remixed, and then resorted at day 2. Differences between weakly and strongly adherent populations were assessed by two-tailed unpaired t-test (n=3). (B) Adherent cells post-sort were cultured in high cations for 3, 6, 11, and 14 days and resorted. Cells that detached were cultured in high cations or low cations mirroring stroma prior to re-sorting. Differences between weakly and strongly adherent populations as a function of culture time and condition were assessed by two-way ANOVA with Tukey test for multiple comparisons (n=3). For time and condition, ANOVA showed ***p<0.001 and ****p<0.0001, respectively as indicated at the corner of the plot. Individual comparisons to their counterpart cation conditions are indicated in the plot with †p<0.1, and *p<0.05. (C) Images of cells from the flow-through (detached) and remaining on the plate (adherent) after exposure to shear along with quantification of the percentage of cells that detached relative to plated cells from each line. n=3. ***p<0.001 for two-tailed unpaired t-test between lines. (D) Plot showing the fraction of detached cells from MDA-MB231, MCF7, and MCF10A and their H-Ras transformed counterparts MCF10AT after exposure to 250 dynes/cm^2 of shear stress.
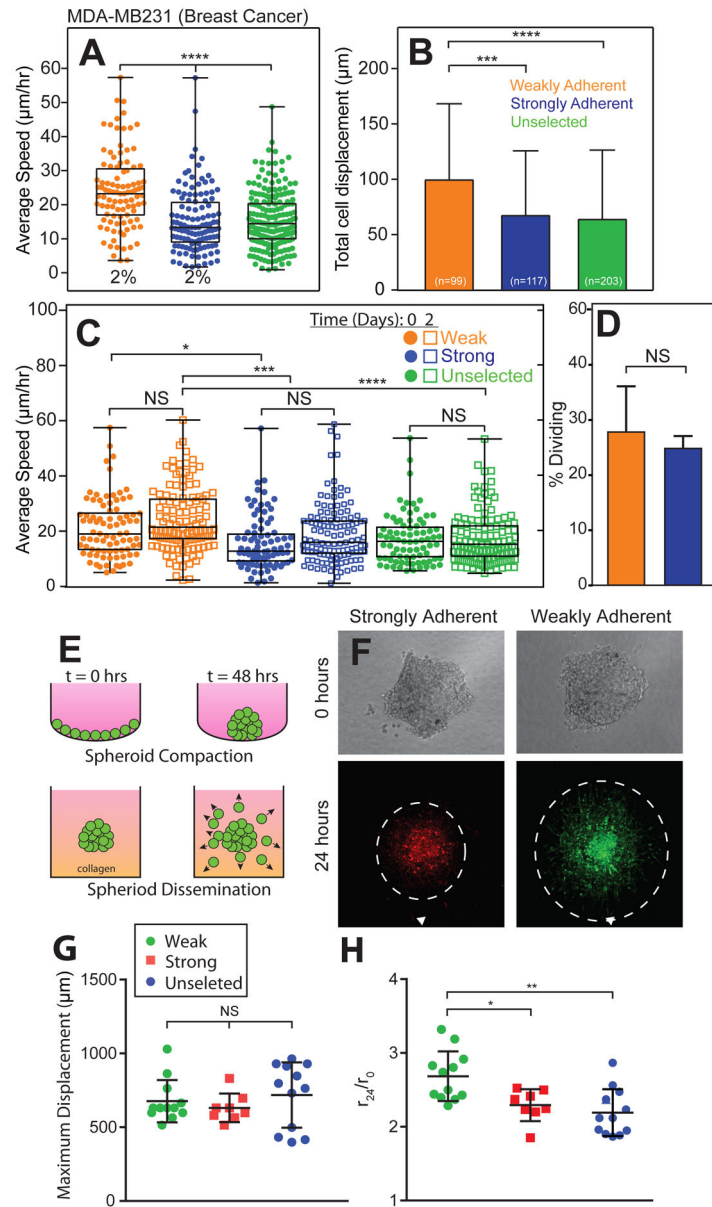
Figure 2: Sorted Populations of Single cells and Spheroids Exhibit and Sustain Different Migration Patterns.

(**A**) Average speed and (**B**) total displacement is plotted for MDA-MB231 cells sorted by the indicated shear stress and allowed to migrate on collagen gels for 24 hours. Percentages in panel A reflect the portion of each population that detaches or remains adherent at a given stress. n=3 biological replicates for the number of cells per condition inset in the bars in panel B. (**C**) Average speed was measured after initial isolation and after 2 days. n=3 biological replicates. (**D**) Plot showing the percentage of dividing cells on a collagen gel over 24 hours for cells selected by the indicated shear stress. n=3 biological replicates. (**E**) Schematic of tumor spheroid formation (top) and subsequent dissemination (bottom) in a collagen gel. (**F**) Brightfield images at the time of spheroid embedding in a collagen gel and fluorescent image 24 hours later. Dashed line indicates the average radius of disseminating

cells. Plots of **(G)** maximum and **(H)** normalized average outward radial migration of cells selected by indicated shear (see Supplemental Figure 5 for radius measurements). One-way ANOVA with Tukey test for multiple comparisons was used to indicate significance where *p<0.05, **p<0.01, ***p<0.001, ***p<0.0001, and N.S. = not significant.
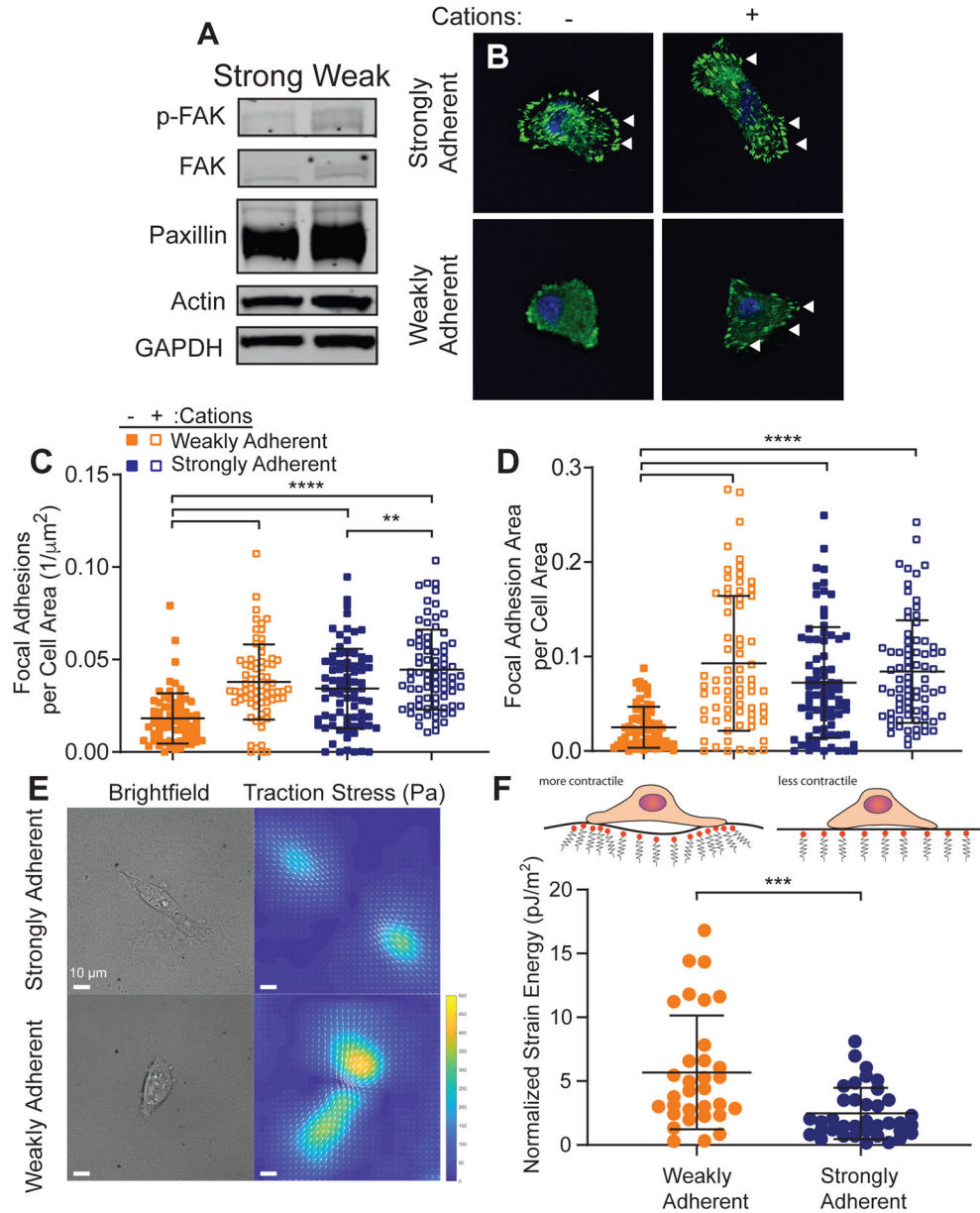
Figure 3: Adherent Phenotypes within a Cancer Line Result from Intrinsic Adhesion Stability and Contractility Differences.

(A) Comparison of the expression of common focal adhesion proteins in strongly adherent (SA) and weakly adherent (WA) cells. (B) Representative images of focal adhesions in SA and WA cells when subjected to with or without cation conditions. (C) Focal adhesion density and (D) total area per cell area is plotted for the indicated sorting and cation conditions. n=3 biological replicates and >50 cells/condition. One-way ANOVA, with Tukey's multiple comparison test was performed for the indicated comparisons with **p<0.01, ***p<0.001, and ****p<0.0001. (E) Brightfield and traction stress plots for cells from the indicated shear conditions. Scale bar is 10 microns. (F) Plot of normalized strain energy for WA and SA cells. n=3 biological replicates and >30 cells/condition. A two-tailed unpaired t-test between lines indicated **p<0.01, ***p<0.001, and ****p<0.0001.

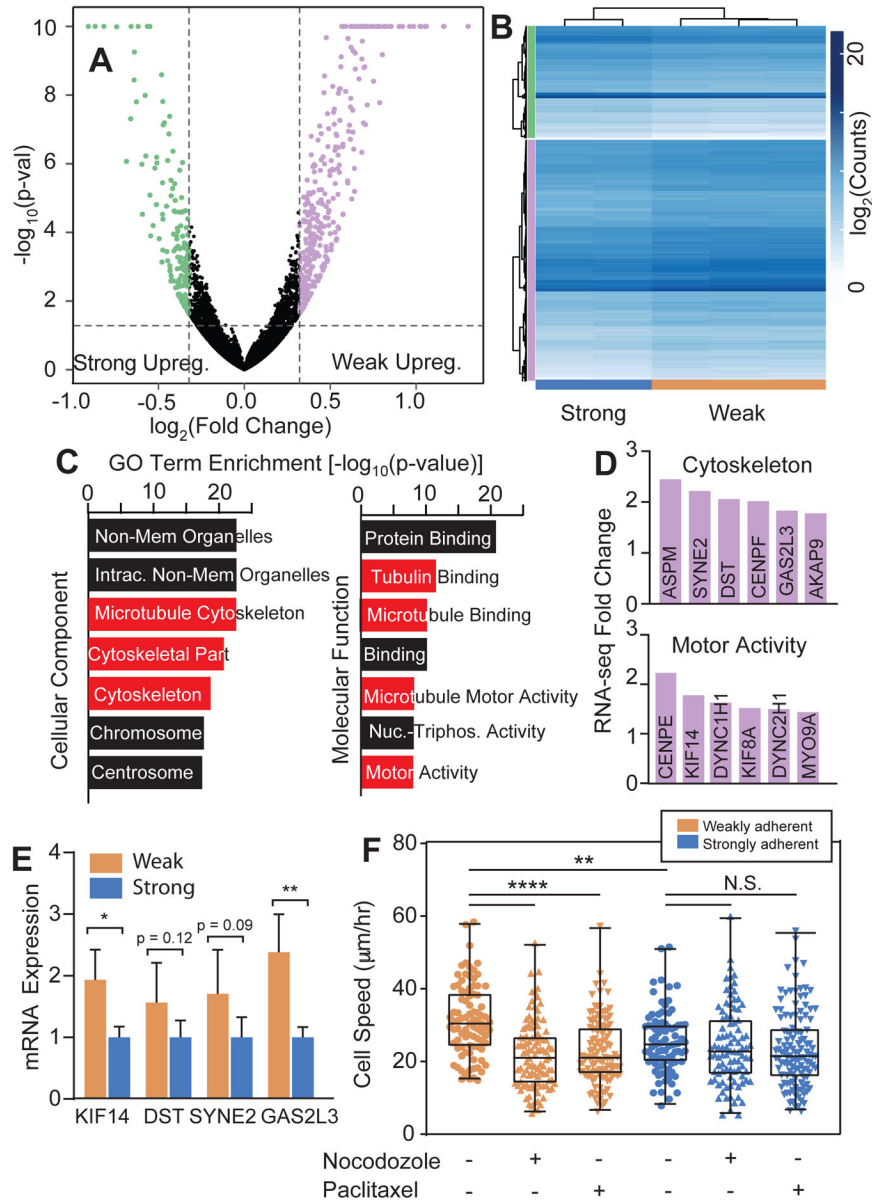**Figure 4: RNA-seq Identifies Intrinsic Patterns that Indicate Structural rather than Expression Changes in Adhesion.**

(A) Differences in gene expression between weakly and strongly adherent MDA-MB231 cells. **(B)** Hierarchical clustering of differentially expressed genes between weakly and strongly adherent cells. Vertical bars indicate clustering of genes that are upregulated in strongly adherent cells and weakly adherent cells. **(C)** Genes ontology terms that are upregulated in the weakly adherent subpopulation. Cytoskeletal and microtubule gene ontology terms, as well as proteins that bind to these components, were significantly upregulated in weakly adherent cells. **(D)** Expressions of genes upregulated in Cytoskeleton and Motor Activity, normalized to strongly adherent subpopulation. **(E)** Validation of RNA seq gene expression differences via qPCR for select genes. *p<0.05 and **p<0.01 for two-tailed unpaired t-test between weakly and strongly adherent cells. **(F)** Average speed of

weakly and strongly adherent cells when treated with microtubule-targeting drugs. At identical concentrations of nocodazole (0.2 ug/mL) and paclitaxel (0.5 ug/mL), weakly adherent cells displayed a significant decrease in migration speed, while the strongly adherent cells demonstrated no change. One-way ANOVA, with Tukey's multiple comparison test was performed for the indicated comparisons with $**p<0.01$, $***p<0.001$, and $****p<0.0001$.
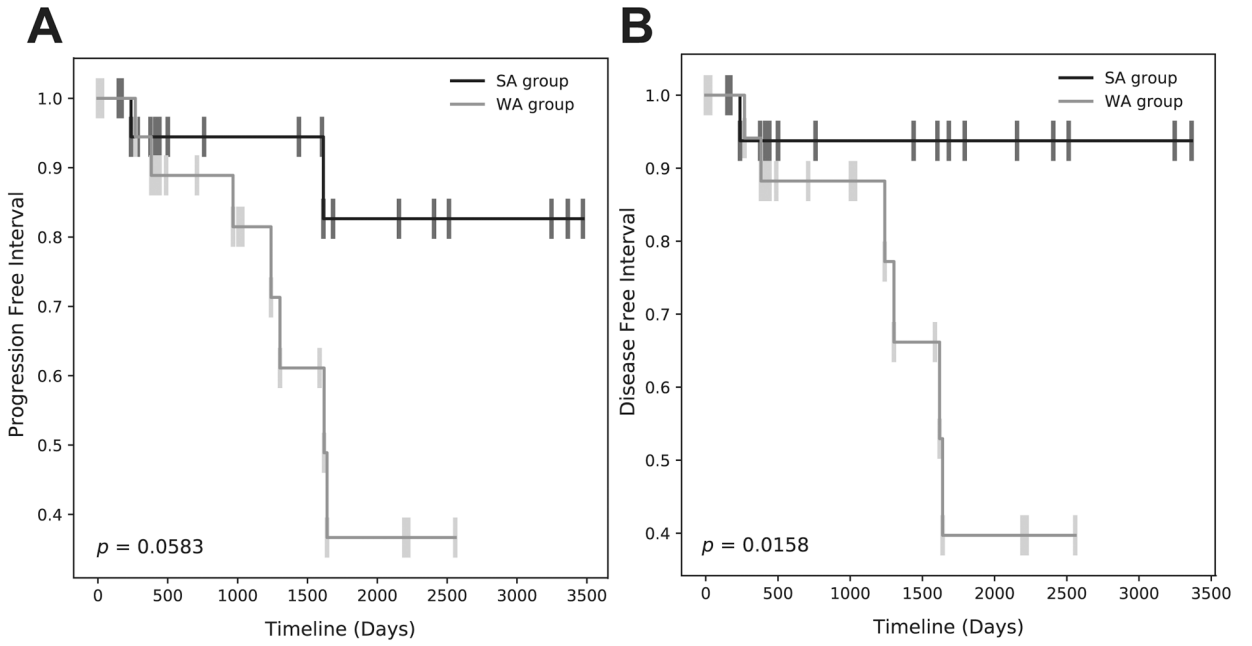
Figure 5: Expression of microtubule-associated genes resembling weakly adherent fraction predicts poor outcome in breast cancer patients.
(A) Progression-free interval and **(B)** disease-free interval of TNBC patients with Stage I-III tumors. Patients with gene expression that resembled strongly adherent and weakly adherent cells were compared. Genes were restricted to those associated with highlighted GO terms in Figure 4C, resulting in a cohort of 100 genes.